
DGGAN: DEGRADATION GUIDED GENERATIVE ADVERSARIAL NETWORK FOR REAL-TIME ENDOSCOPIC VIDEO ENHANCEMENT

Handing Xu, Zhenguo Nie*, Tairan Peng, Xin-Jun Liu

Department of Mechanical Engineering,
State Key Laboratory of Tribology in Advanced Equipment,
Beijing Key Laboratory of Transformative High-end Manufacturing Equipment and Technology
Tsinghua University
Beijing, China

{Handing Xu, Zhenguo Nie}xhd21@mails.tsinghua.edu.cn, zhenguo nie@tsinghua.edu.cn

Huimin Pan

Department of Mechanical Engineering
Tsinghua University
Beijing, China

ABSTRACT

Endoscopic surgery relies on intraoperative video, making image quality a decisive factor for surgical safety and efficacy. Yet, endoscopic videos are often degraded by uneven illumination, tissue scattering, occlusions, and motion blur, which obscure critical anatomical details and complicate surgical manipulation. Although deep learning-based methods have shown promise in image enhancement, most existing approaches remain too computationally demanding for real-time surgical use. To address this challenge, we propose a degradation-aware framework for endoscopic video enhancement, which enables real-time, high-quality enhancement by propagating degradation representations across frames. In our framework, degradation representations are first extracted from images using contrastive learning. We then introduce a fusion mechanism that modulates image features with these representations to guide a single-frame enhancement model, which is trained with a cycle-consistency constraint between degraded and restored images to improve robustness and generalization. Experiments demonstrate that our framework achieves a superior balance between performance and efficiency compared with several state-of-the-art methods. These results highlight the effectiveness of degradation-aware modeling for real-time endoscopic video enhancement. Nevertheless, our method suggests that implicitly learning and propagating degradation representation offer a practical pathway for clinical application.

Keywords Real-time Video enhancement · Degradation representation · Cyclical consistency · Endoscopic video

1 Introduction

Minimally invasive surgery (MIS) has become a cornerstone of modern clinical practice, offering reduced surgical trauma, shorter recovery times, and improved postoperative outcomes compared with traditional open procedures. Among various MIS techniques, endoscopic surgery plays a particularly critical role, as it enables surgeons to access deep or delicate anatomical regions through narrow working channels with minimal disruption of surrounding tissues. For example, in spine surgery, endoscopic approaches have been increasingly adopted for the treatment of conditions such as lumbar disc herniation, spinal stenosis, and degenerative diseases[1]. Unlike open spine procedures, spine endoscopy relies entirely on intraoperative video as the sole source of visual feedback, making video quality a decisive factor for surgical safety and efficacy.

*Corresponding author

However, endoscopic videos are often far from ideal. The imaging environment inside the human body presents a variety of challenges: illumination is highly non-uniform due to directional light sources; optical scattering by tissues and fluids degrades image contrast; blood, smoke, and surgical instruments frequently occlude the field of view; and camera motion or limited depth of field can introduce blur. These degradations collectively compromise the visibility of fine anatomical structures, hinder accurate surgical manipulation, and may increase the risk of complications. In spine endoscopy, where the operative corridor is typically only a few millimeters in diameter and critical neural structures lie in close proximity, such limitations become particularly critical. Even subtle degradations in video clarity can obscure vital anatomical cues and complicate intraoperative decision-making.

To address these challenges, video enhancement techniques have been widely investigated. Conventional approaches [2, 3, 4, 5] can provide modest improvements in brightness or contrast, but they often fail under severe degradations and may amplify noise or introduce artifacts [6]. More recently, deep learning-based methods have demonstrated remarkable success in image restoration tasks, including denoising, deblurring [7], and super-resolution [8, 9], by leveraging large-scale data and learning complex degradation models. These techniques have been gradually extended to the domain of endoscopic imaging, with promising results in improving surgical visibility.

Nevertheless, several critical limitations remain. Most existing methods are designed and evaluated in offline settings, where computational efficiency is not a primary concern. As a result, they often involve complex models or iterative optimization procedures that are computationally expensive and unsuitable for deployment in the operating room. In real surgical environments, enhancement must be performed at video frame rates to provide surgeons with immediate visual feedback. The inability of current methods to achieve real-time restoration therefore represents a substantial barrier to clinical adoption.

In this work, we propose a real-time enhancement framework for endoscopic videos. We begin by designing a degradation-aware module that estimates an implicit representation of the degradation present in the current frame. Building on this representation, we develop a generative single frame enhancement model that trains in a cyclical-consistent manner by degrading the restored image. Furthermore, based on the hypothesis that image degradations typically evolve continuously during most surgical procedures, we introduce a Transformer-based degradation propagation module that predicts the degradation representation of subsequent frames from previous ones. This design enables the model to directly estimate degradation characteristics only at regular intervals, substantially reducing inference time and making high-quality real-time enhancement of endoscopic videos feasible. Qualitative and quantitative comparisons with other video or image enhancement methods demonstrate the superior performance and efficiency of the proposed method in enhancing endoscopic videos. Our contributions can be summarized as follows:

- **Inter-frame degradation representation propagation:** We proposed a mechanism that propagates degradation representations across frames, enabling real-time video enhancement while maintaining high-quality outputs.
- **Single frame enhancement model:** We design a single-frame image enhancement model that leverages cyclical consistency to achieve high-quality training.
- **Degradation representation fusion mechanism:** We introduce a fusion strategy that modulates image features with degradation representations, facilitating degradation-guided feature generation and enhancement.

2 Related work

2.1 Endoscopic video enhancement

The enhancement of endoscopic video streams is a critical research area focused on correcting dynamic degradations to provide a clear and stable view for clinicians. Algorithmic solutions primarily target motion blur and various visual artifacts that compromise video quality. Early methods that processed each frame independently were often insufficient, as they failed to account for the temporal nature of video, leading to inconsistencies and suboptimal results. Consequently, modern research heavily utilizes the temporal context available in video sequences. For instance, in addressing motion blur caused by physiological movement or instrument instability, synthesis-based methods have proven effective. These techniques restore sharpness in blurred frames by identifying and transferring high-frequency details from adjacent clear frames, a process demonstrated by [10] using a non-parametric motion model to align the frames accurately.

The advent of deep learning has also marked a paradigm shift in handling image artifacts. Of the various artifacts that degrade endoscopic images, specular reflections are particularly problematic, as they can saturate parts of the image and obscure critical underlying tissue. While traditional methods relied on filtering and inpainting, deep learning models can now intelligently detect these highlights and reconstruct the missing information. Beyond reflections, these models have excelled at removing other common obstructions. The field has evolved from physics-based models, such as

the chromaticity-based approach for smoke removal proposed by [11], to more advanced deep learning solutions like improved U-Net architectures that perform real-time desmoking [12]. Furthermore, to combat the inherent noise in endoscopic sensors, CNN-based blind denoising methods have been developed to handle noise without requiring prior information about its statistical properties [13, 14]. Other specialized models effectively eliminate bubble artifacts in wireless capsule endoscopy videos, which frequently obstruct the view of the gastrointestinal tract [15].

2.2 Real-time image enhancement

Real-time image enhancement provides immediate visual improvement during live procedures, a crucial capability for on-the-fly diagnosis and intervention. This domain is now dominated by deep learning models that offer both the rapid processing speed and the sophisticated analytical power required for clinical application. Super-resolution (SR) is a vital technique for improving detail from low-resolution sources, such as capsule endoscopes, or for reducing bandwidth requirements in video streaming. The field has progressed rapidly from foundational CNNs to advanced architectures. Modern models like EndoL2H use Generative Adversarial Networks (GANs) and spatial attention mechanisms to generate high-fidelity, photorealistic images [16]. The latest trend involves hybrid models that combine CNNs with transformers to capture both local textural features and long-range contextual dependencies, as seen in HA-VSR [17] and E-SEVSR [18]. Additionally, saliency-aware and attention mechanisms are being integrated to focus computational resources on diagnostically relevant regions, further boosting performance and efficiency [19, 20].

For low-light conditions that can obscure critical anatomical features, Retinex-based deep networks like EIEN have been developed to correct illumination while preserving natural colors and details [21]. Unsupervised models such as EnlightenGAN offer greater flexibility by not requiring paired training data, which is often difficult to acquire in medical settings [22]. Beyond improving raw image quality, deep learning powers real-time computer-aided detection (CADE) and diagnosis (CADx) systems. Functioning as a "second observer," these systems highlight suspicious areas for clinicians. CNN models can detect and classify pathologies like polyps and early-stage cancers in video streams at speeds exceeding 25 frames per second, well within the requirements for real-time clinical use [23, 24]. Recent advancements include multi-task models like DSI-Net for joint classification and segmentation [25] and robust ensemble learning techniques that improve accuracy and reliability by combining predictions from multiple models [26, 27].

3 Methodology

3.1 Video enhancement framework

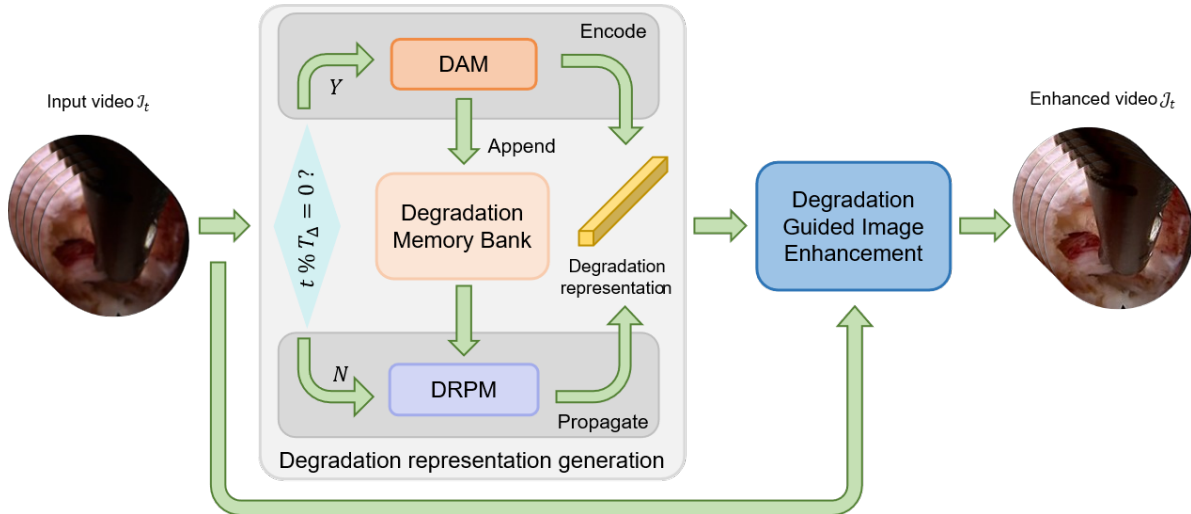


Figure 1: Framework of the real-time video enhancement. Each frame of the input video sequence undergoes degradation representation modeling and enhancement generation. Specifically, for frames whose index is a multiple of T_{Δ} , the system invokes the degradation-aware module (DAM) to perform a full estimation, yielding high-precision degradation features. For frames that are not multiples of T_{Δ} , the degradation representation is rapidly propagated through the degradation representation propagation module (DRPM) along the temporal dimension and subsequently fed into the single frame enhancement model to enhance the current frame. All the modules are detailed in the following sections.

The proposed endoscopic video enhancement framework is illustrated in Fig. 1. In this framework, each frame of the input video sequence undergoes degradation representation modeling and enhancement generation. Specifically, for frames whose index is a multiple of Δ_T , the system invokes the degradation-aware module to perform a full estimation, yielding high-precision degradation features. For frames that are not multiples of Δ_T , the degradation representation is rapidly estimated through the DRPM along the temporal dimension and subsequently fed into the generator to enhance the current frame.

This “key-frame—propagated-frame” design enables the framework to maintain accurate degradation representations without performing high-complexity modeling on every frame, thereby significantly reducing the overall computational load. More importantly, the propagation mechanism ensures strong temporal consistency and continuity across the video sequence, allowing the system to produce stable enhancement results while satisfying real-time requirements. Such a design lays the foundation for online enhancement applications in clinical surgical scenarios.

3.2 Single frame enhancement model

We introduce a single-frame image enhancement model that is guided by degradation representation. Building upon the CycleGAN framework [28], our approach leverages cyclical consistency between degraded and restored images to construct the training paradigm. Within the generator, we design a dedicated degradation-aware module (DAM) to extract the implicit degradation characteristics of the input image, which are then used to guide the enhancement of the current frame. This design ensures that the enhancement process is explicitly aware of image degradation, leading to more reliable restoration in complex surgical scenarios.

3.2.1 Degradation-aware module

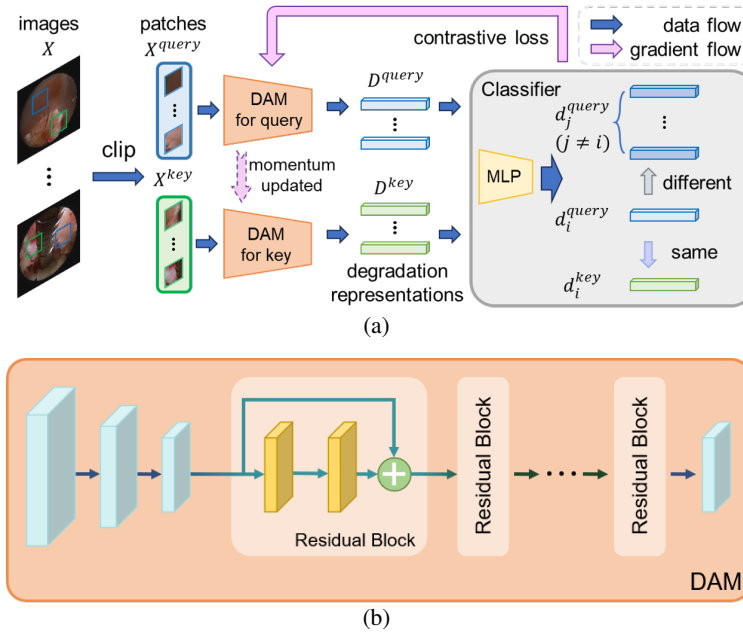


Figure 2: The diagram of the DAM. (a) The DAM training workflow. (b) The structure of the DAM.

This module learns to characterize degradation representations through a contrastive learning strategy inspired by MoCo [29, 30]. As illustrated in Fig. 2(a), given a batch of N images X , the assumption is that only representations extracted from the same image should be identical, while those from different images should remain distinct. To enforce this property, the degradation-aware module is trained using the InfoNCE loss [31] as (1), which measures the similarity among multiple degradation representations.

$$L_{\text{con}} = -\log \frac{\exp(d_i^q \cdot d_i^k / \tau)}{\sum_{j=1}^N \exp(d_i^q \cdot d_j^k / \tau)} \quad (1)$$

To strengthen the expressive capacity of the DAM, we replace conventional stacked convolutional layers with a series of residual blocks, as shown in Fig. 2(b). This architectural refinement allows the encoder to capture richer and

more discriminative degradation features. Importantly, by producing a more accurate and compact representation of degradation, the DAM reduces the burden on the subsequent image enhancement module. As a result, the overall framework not only improves the quality of degradation modeling but also lowers the complexity of the enhancement stage, which is essential for achieving real-time endoscopic video enhancement.

3.2.2 Degradation guided enhancement module

As shown in Fig. 3(a), building on the degradation representation generated by the DAM, we design an degradation guided enhancement module (DGEM) that generates enhanced image in four sequential stages.

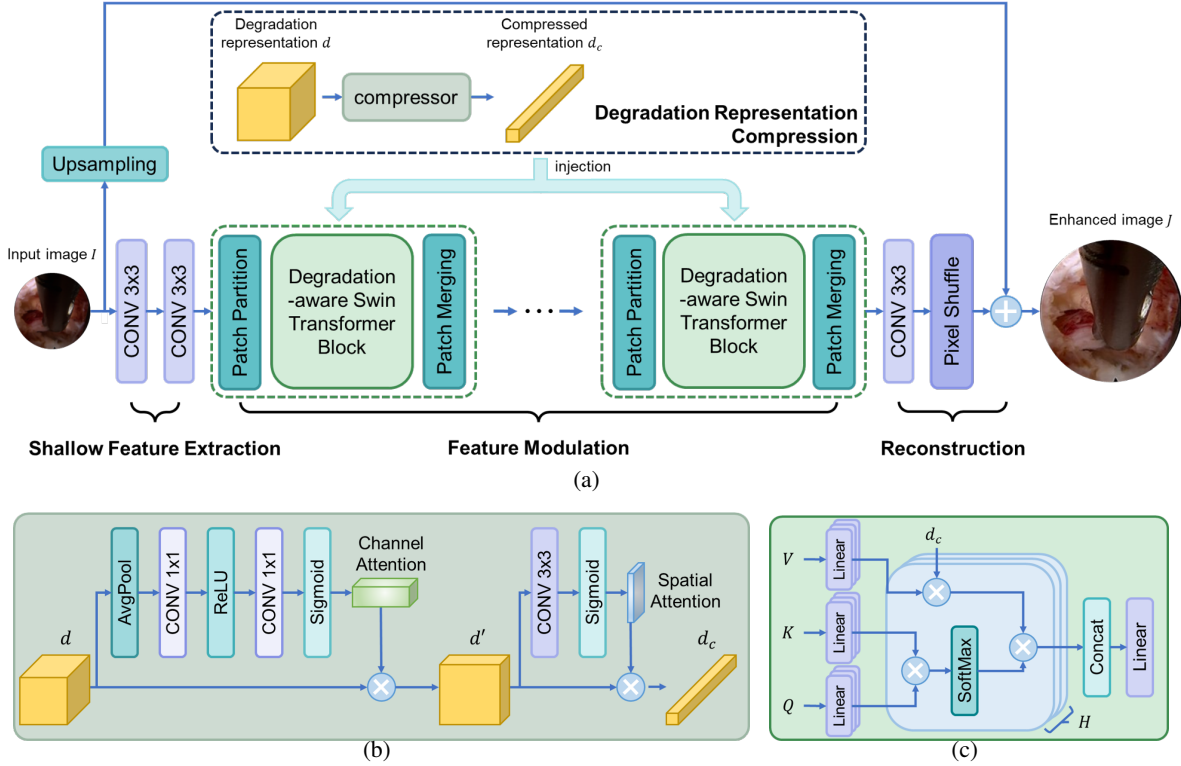


Figure 3: Degradation guided enhancement module (DGEM). (a) The basic architecture of the DGEM, which includes four parts: Degradation representation compression, shallow feature extraction, feature modulation, and Reconstruction. (b) The degradation compression block, which implements both channel attention and spatial attention mechanisms. (c) The Degradation-aware Swin Transformer Block, which injects the degradation representation d_c into the value component and modulates the input feature based on multi-head self-attention.

Degradation representation compression. The extracted degradation representation d is high-dimensional and often redundant. To obtain a compact yet informative embedding, we introduce both channel attention and spatial attention mechanisms as (2), which selectively emphasize the most relevant degradation cues while suppressing irrelevant information (Fig. 3(b)).

$$\begin{aligned} d' &= \sigma(W_{c2}\delta(W_{c1}d)) * d \\ d_c &= \sigma(W_{s1}d') * d' \end{aligned} \quad (2)$$

where σ, δ represent the sigmoid and ReLU activation function separately.

Shallow feature extraction. We extract low-level structural information from the input image using two stacked 3×3 convolutional layers. This step preserves local edges and textures, which are essential for fine-grained restoration.

Feature modulation. Inspired by the Swin Transformer [32], we adopt a shifted-window attention mechanism to capture both local and long-range dependencies. Building upon the standard multi-head attention mechanism, we introduce a degradation-aware modulation applied specifically to the value vectors in each attention head, as shown in

Fig. 3(c). As shown in (3), by incorporating the degradation representation into the values, the attention module can adaptively emphasize or suppress features according to the estimated degradation in the input image.

$$\begin{aligned} \hat{V} &= V \odot d \\ \text{MSA}(I) &= [\text{Concat}_{h=1}^H(\text{Softmax}(\frac{Q_h K_h^T}{\sqrt{d_h}})\hat{V})]W_o \end{aligned} \quad (3)$$

where d denotes the compressed degradation representation, Q_h , K_h , and V_h correspond to the query, key, and value of the h -th attention head, and d_h represents the dimensionality of each head.

Unlike modulating the query or key vectors, which would alter the attention distribution itself, modulating the Values directly adjusts the content carried through the attention mechanism, allowing the network to integrate degradation information without disrupting spatial relationships. This strategy enables more effective feature aggregation that is guided by the current degradation conditions, ultimately improving the fidelity and robustness of the enhanced image.

Reconstruction. Finally, the modulated features are passed into a sub-pixel convolution upsampling module, which ensures that the final output benefits from degradation-aware guidance while maintaining high spatial fidelity.

3.2.3 Cyclical consistency

In the CycleGAN framework, style transfer between two image domains is achieved by employing two generators and two discriminators under the constraint of cyclical consistency. Inspired by this idea, we construct a cyclical consistent adversarial network between the low-quality and high-quality image domains, denoted as \mathcal{L} , \mathcal{H} , respectively. As illustrated in Fig. 4(a), the enhancement process $\mathcal{L} \rightarrow \mathcal{H}$ is carried out by the DAM and the DGEM, while the degradation process $\mathcal{H} \rightarrow \mathcal{L}$ is directly implemented based on predefined degradation models (PDMs).

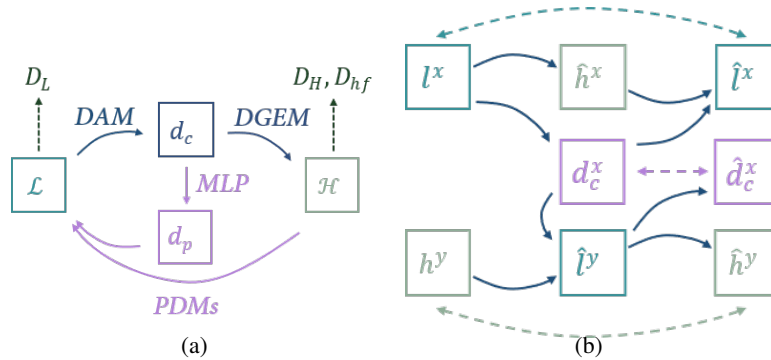


Figure 4: Diagram of the cyclical consistency. (a) The dataflow of the whole model. $\mathcal{L} \rightarrow \mathcal{H}$: achieved by the DAM and the DGEM with an additional output d_c . $\mathcal{H} \rightarrow \mathcal{L}$: achieved based on PDMs and the regression of d_p . (b) Calculation of the cyclical consistency loss. Solid lines indicate the dataflow when generating reconstructed synthetic images, and dashed lines indicate the cyclical consistency loss calculation at both ends.

For the degradation process $\mathcal{H} \rightarrow \mathcal{L}$, as shown in the purple part in Fig. 4(a), multiple lightweight degradation parameter regression modules based on different predefined image degradation models. This module estimates explicit degradation parameters d_p from the learned implicit degradation representation, which are then used to synthesize degraded images back. Taking the classical image blurring model $\hat{\mathcal{I}} = \sigma \otimes \mathcal{I} + n$ as an example, the regression module can estimate a spatially varying blur kernel $\hat{\sigma}_{i,j}$ together with a noise intensity field $\hat{n}_{i,j}$. These estimated parameters are further used to degrade the enhanced images back to the low-quality domain \mathcal{L} , thereby enabling training with paired high- and low-quality images. Importantly, by grounding the degradation process in physically meaningful models rather than in an unconstrained learned generator, our framework avoids introducing unrealistic artifacts and ensures that the cyclical consistency better reflects the actual imaging degradation.

In the style of CycleGAN, generator G and the degradation model D aim to produce synthetic high-quality and low-quality images, respectively, whereas the appearance discriminators D_L, D_H compete with the corresponding generators to correctly differentiate the synthetic images from the real images, denoted by (4) and (5). For simplicity, we use G_H to denote the combination of DAM and DGEM, and G_L to denote PDMs. To encourage the generation of high-quality enhanced images, we extend the standard two-discriminator framework by adding a high-frequency

discriminator D_{hf} that focuses specifically on the high-frequency of the high-quality image domain. This design aims to guide the generator in preserving fine-grained details and texture information, and its corresponding adversarial loss is defined as (6).

$$L_{adv}(G_H, D_H) = \mathbb{E}_{x_h \sim p(x_h)} [\log(D_H(x_h))] + \mathbb{E}_{x_l \sim p(x_l)} [\log(1 - D_H(G_H(x_l)))] \quad (4)$$

$$L_{adv}(G_L, D_L) = \mathbb{E}_{x_l \sim p(x_l)} [\log(D_L(x_l))] + \mathbb{E}_{x_h \sim p(x_h)} [\log(1 - D_L(G_L(x_h)))] \quad (5)$$

$$L_{adv}(G_H, D_{hf}) = \mathbb{E}_{x_h \sim p(x_h)} [\log(D_{hf}(F_{hp}(x_h)))] + \mathbb{E}_{x_l \sim p(x_l)} [\log(1 - D_{hf}(F_{hp}(G_H(x_l))))] \quad (6)$$

where F_{hp} denotes a highpass filter.

As shown in Fig. 4(b), the cyclical consistency loss is defined as (7), which forces the reconstructed synthetic images $G_L(G_H(L))$ and $G_H(G_L(H))$ to be identical to their respective inputs L and H .

$$L_{cyc}(G_H, D) = \mathbb{E}_{x_l \sim p(x_l)} [\|G_L(G_H(x_l)) - x_l\|_1] + \mathbb{E}_{x_h \sim p(x_h)} [\|G_H(G_L(x_h)) - x_h\|_1] + \mathbb{E}_{x_l, x_h \sim p(x_l), p(x_h)} [\|D(G_L(x_h)) - D(x_l)\|_1] \quad (7)$$

where the third term denotes the cyclical consistency of the degradation representation, and D in it represents the DAM. It should be mentioned that the degradation representation d_c can be only produced by the DAM within G_H . Consequently, in the term $G_L(x_h, d_c^h)$, the degradation representation d_c^h can only be replaced with d_c^l that derived from $G_H(x_l)$, which means that the degradation representation cycle contains only a single term.

3.3 Degradation representation propagation module

Although the aforementioned single-frame image enhancement model can achieve high-quality endoscopic image restoration, its inference efficiency is insufficient to meet the real-time requirements of intraoperative observation. To address this, we balance the complexity of different model components against overall performance. Specifically, we manually adjust the number of residual blocks and Swin Transformer blocks to adjust the number of parameters and floating-point operations (FLOPs) for each module (detailed in Table 1), concentrating the primary computational cost in the degradation representation extraction stage.

Table 1: Number of parameters and FLOPs for each part of DGGAN.

	Params(M)	GFLOPs
DAM	4.33	29.75
DGEM	0.39	24.65
Degradation Representation	0.066	1.31
Compression		
Shallow Feature Extraction	0.0018	0.11
Feature Modulation	0.13	8.22
Reconstruction	0.19	15.01

Based on these adjustments, we further introduce a degradation representation propagation module (DRPM) to fully exploit temporal correlations across video frames. This module leverages the degradation representations of previous frames as implicit priors, propagating and updating them along the temporal dimension to efficiently estimate the degradation representations of future frames. Compared with modeling each frame independently, this propagation mechanism significantly reduces redundant computations by avoiding repeated processing of highly similar information across adjacent frames, thereby lowering overall computational complexity and ensuring real-time enhancement. Moreover, by maintaining inter-frame consistency of the degradation representations, the module enhances the stability and temporal coherence of degradation modeling across sequences.

In implementation, the DRPM is built upon a Transformer architecture as shown in Fig. 5. Unlike conventional recurrent neural networks (RNNs) or 3D convolutional networks (3D-CNNs), the self-attention mechanism in Transformers enables flexible modeling of dependencies over a long temporal range, overcoming the locality constraints of convolution or the limited temporal span of RNNs. Through multi-head attention, the module can simultaneously capture multi-scale temporal correlations in the degradation representations, accurately modeling both local dynamics between adjacent frames and long-range dependencies across distant frames. As a result, employing a Transformer not only improves the accuracy and robustness of degradation representation estimation but also preserves temporal consistency and overall stability in the enhanced video sequence.

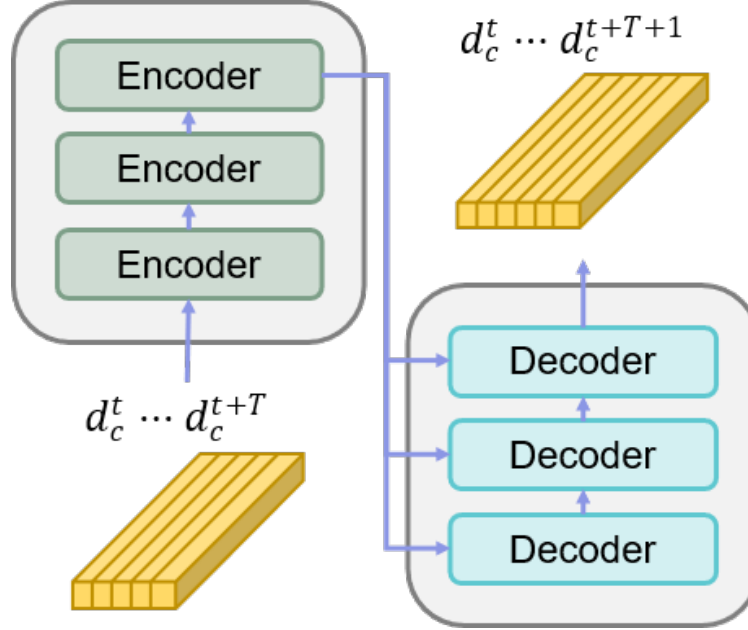


Figure 5: The architecture of the DRPM.

Importantly, to further improve the efficiency of degradation propagation while maintaining effectiveness, the module does not propagate the full degradation representation D directly. Instead, it uses a compressed representation \hat{D} as the temporal modeling unit, which is not directly illustrated in Fig. 1. This strategy reduces feature dimensionality and computational redundancy, while also enhancing the model’s generalization and real-time performance, providing an efficient degradation-aware support for continuous-frame endoscopic image enhancement.

3.4 Training strategy

The training strategy is detailed in Algorithm 1. In first N_d epochs, the model first pre-trains the DAM using the contrastive loss L_{con} on paired endoscopic images generated by artificial degradations, enabling it to capture effective degradation representations. After this stage, we switch to real-world data, training the model on unpaired low-quality and high-quality endoscopic images under the CycleGAN paradigm. During adversarial learning, to train the generators, the associated objective is minimized while to train the discriminators, the associated objective is maximized. Please note that when the generators are optimized, the weights of the discriminators are fixed and vice versa. At each step, we conduct following computations including forward propagation, loss calculation, backward propagation and updating weights of associated components. Finally, for video datasets, non-key frames are processed by replacing the DAM in the single-frame enhancement model with the DRPM. The training is then conducted using the same loss functions as described above, which guide the DRPM to propagate and generate reasonable degradation representations.

The design of this two-stage dataset utilization scheme is motivated by two key considerations. On one hand, acquiring large-scale paired endoscopic data in clinical practice is extremely challenging, particularly for image pairs exhibiting diverse degradation types, which has a significant impact on the generalization capability of the DAM. On the other hand, models trained solely on artificially degraded pairs often generalize poorly to real surgical videos. By first initializing the degradation representation module with artificial pairs and then adapting the whole model with real unpaired data, our approach combines the advantages of both worlds and ensures better performance in realistic surgical environments.

Algorithm 1: Training strategy

Input: A dataset of high quality endoscopic images X_h , A dataset of low quality endoscopic videos X_l , A predefined degradation model PDM

```

1 for epoch in  $0, N_d$  do
2   Sampling  $x_h$  from  $X_h$ 
3   Generate  $\hat{x}_l$  by degrading PDM( $x_h$ )
4   Train DAM by minimizing  $L_{con}$ 
5 end
6 for epoch in  $N_d, N_d + N_s$  do
7   Sampling  $x_h$  from  $X_h$ 
8   Sampling  $x_l$  from  $X_l$  as images
9   Train  $G_L, G_H$  by minimizing  $L_{adv} + L_{cyc}$ 
10  Train  $D_L, D_H, D_{hf}$  by maximizing  $L_{adv}$ 
11 end
12 for epoch in  $N_d + N_s, N$  do
13   Sampling  $x_h$  from  $X_h$ 
14   Sampling  $x_l^t, \dots, x_l^{t+T}$  from  $X_l$  as videos
15   Replace DAM with DRPM
16   Train DRPM by minimizing  $L_{adv} + L_{cyc}$ 
17   Train  $D_L, D_H, D_{hf}$  by maximizing  $L_{adv}$ 
18 end

```

4 Experiments and results

In this section, we first evaluate the performance of the proposed method on the SCARED dataset [33] and compare it with several state-of-the-art deep learning-based approaches. We then assess the degradation-awareness capability of the proposed module, demonstrating the effectiveness of the learned degradation representations. Furthermore, we evaluate the performance of our method under different degradation patterns across various surgical scenarios. To gain deeper insights into the contribution of each component, we conduct ablation studies. Finally, we construct a simulated surgical environment to examine the real-time performance of the proposed approach. Code is available at: <https://github.com/ilk123/DGGAN>.

4.1 Data collection and implementation details

4.1.1 Datasets and preprocessing

In this study, we construct two datasets to support model training and evaluation. For the high-resolution images, we adopt the SCARED dataset. Although originally designed for monocular depth estimation, we select 2, 295 clear and high-quality left-camera images to build a high-quality endoscopic image dataset. For the low-resolution videos, we utilize the spinal endoscopic surgery dataset (referred as the SES dataset) collected at Peking University People's Hospital, from which we extract 240 clips, each consisting of 120 frames. The choice of this dataset is motivated by the fact that Percutaneous Endoscopic Lumbar Discectomy (PELD) is performed in a narrow operative field filled with irrigation fluid and image is degraded severely, which may post different levels of challenge to our method.

Specifically, the resolution of the SCARED dataset is 1280×1024 , while the spinal endoscopic dataset has resolutions of 720×1080 or 1920×1080 . In order to reduce the redundant areas of the images, such as pure black areas and inner wall of the working channel, we crop the images into 320×320 patches to construct the low-quality endoscopic dataset. Finally, the SCARED dataset and the SES dataset are split into training, validation, and testing sets following a 7:2:1 ratio.

4.1.2 Implementation details

We train our model following the procedure outlined in Algorithm 1. Throughout the training process, we adopt the Adam optimizer with parameters set to $\beta_1 = 0.9$ and $\beta_2 = 0.999$. During the training of the DAM, the learning rate is set to $5e - 5$. For the training of the single-frame enhancement model, the learning rate of G and D are set to $5e - 5$ and $2e - 4$, separately. For the DRPM, we configure the time interval for DAM-based degradation estimation to 15 frames,

with the same learning rate as the previous stage. All experiments are conducted using two NVIDIA RTX 3090Ti GPUs for training, while a single NVIDIA RTX 3090Ti is employed for model testing.

4.2 Enhancement performance and efficiency of DGGAN

We compare our method with several open-source image enhancement algorithms, including degradation-specific approaches as well as two general-purpose methods (Restormer [34] and SwinIR [35]). For our framework, we evaluate both the two variants: the degradation-guided enhancement model based on DAM (DGGAN-DAM) and the degradation-guided enhancement model based on DRPM (DGGAN-DRPM).

We first conduct experiments on the SCARED dataset, where the low-quality test images are generated by applying degradations based on multiple degradation models, as defined below. Since the ground truth is available in this setting, we adopt PSNR [36] and SSIM [37] as full-reference metrics to evaluate image quality. We then conduct experiments on the spinal endoscopic dataset, where no ground truth is available. In this case, we employ no-reference metrics, including NIQE [38] and PIQE [39], to assess the performance of different models.

In addition, to evaluate the computational efficiency of each model, we reported two key complexity measures-the number of parameters and the floating point operations (FLOPs)-following common practice in super-resolution studies. To measure the computational efficiency of each model, we calculate two essential properties: the number of parameters and FLOPs (Floating-point operations per second). The number of parameters in a model describes its size, with fewer parameters indicating a more lightweight model. FLOPs can describe the computational complexity of the model, and have become a widely used metric to measure the efficiency of models.

4.2.1 Degradation models

On the SCARED dataset, we apply four degradation types frequently observed in endoscopic surgery: noise, motion blur, low illumination, and electrocautery smoke. For each type, the corresponding degradation model is implemented as summarized in Table 2, and during the training of our DGGAN model, the associated parameters are regressed to support the degradation process.

Table 2: The corresponding models for different degradation types.

Degrade Type	Degrade Model
Random Noise	$I(x) = J(x) + n(x)$
Motion Blur	$I(x) = k(x) \otimes J(x)$
Low Light	$I(x) = J(x) \cdot L(x) + n(x)$
Smoke	$I(x) = J(x)t(x) + A(1 - t(x))$
SES	referred as to (8)

It should be mentioned that although explicit degradation models and their parameters are calculated, we deliberately choose not to use these parameters as direct supervision signals. Instead, our framework learns to encode and exploit degradation representations that implicitly capture the degradation characteristics. This design enables the model to move beyond parameter-specific regression and achieve greater robustness and generalization across diverse degradations.

For the spinal endoscopy dataset, we further construct a degradation representation model (8) tailored to real surgical scenarios, taking into account four major aspects: low resolution, blurring, low illumination, and underwater imaging effects.

$$I(x) = (\beta(\alpha J(x) \otimes k)^\gamma T(x) + A(1 - T(x))) \downarrow_s + n \quad (8)$$

4.2.2 Results on SCARED dataset

The performance of multiple models on SCARED dataset are shown in Table 3 and Fig. 6. It is worth noting that since our DGGAN framework incorporates an inherent super-resolution step, for competing methods without a upsampling module, we adopt a strategy of first applying enhancement and then bicubic interpolation for resolution restoration. While this inevitably reduces their final performance, it keeps their inference efficiency comparable.

For the denoising task, we compare against DnCNN [40], CBDNet [41], and Uformer [42]. As denoising represents the simplest enhancement scenario, the performance of all models is remarkable except DnCNN, since it was trained for Grayscale image denoising. Notably, our DGGAN-DRPM achieves results only slightly lower than Restormer and SwinIR, while requiring just 30% and 7.3% of their FLOPs, respectively.

For the deblurring task, we select DeblurGAN [43], MIMOUNet [44], and DBGAN [45]. In this case, DGGAN-DAM achieve the best overall performance, surpassing Restormer by 0.1083 in SSIM, while DGGAN-DRPM reaches 0.7785 SSIM, ranking just behind DGGAN-DAM and SwinIR.

For the low-light enhancement task, we compared against Zero-DCE [46], RetinexNet [47], and EnlightenGAN [22]. Here, DGGAN-DAM nearly matches Restormer’s performance (a marginal SSIM drop of 0.0038), while DGGAN-DRPM ranks third overall, outperforming SwinIR by 0.0327.

For the electrocautery smoke removal task, we selected DehazeNet [48], FFANet [49], and MSBDN [50]. Again, DGGAN-DAM achieves the best results, though DGGAN-DRPM underperforms compared to Restormer and SwinIR. We attribute this to the inherently stochastic nature of smoke diffusion, which limits the ability of the DRPM to effectively propagate degradation representations across frames.

Overall, these results highlight that even when compared against task-specific enhancement models under comparable efficiency settings, our framework consistently achieves an outstanding balance between computational efficiency and enhancement quality. In particular, for each degradation type, we deliberately choose relatively lightweight baseline models to ensure similar inference efficiency, thereby making the performance gains of our method more directly attributable to its superior balance between efficiency and effectiveness.

4.2.3 Results on SES dataset

We conduct evaluations on our SES dataset subsequently. Although the performance can only be assessed using no-reference quality metrics, specifically NIQE and PIQE, the results in Table 4 and Figure 6 clearly demonstrate that our method significantly outperforms both Restormer and SwinIR. This finding highlights the strong capability of DGGAN in handling complex and diverse degradation scenarios. More importantly, in real surgical environments, the challenges differ markedly from those in general image enhancement tasks. While patient-specific anatomical and physiological conditions may vary, the types of visual degradations that occur during a given minimally invasive surgery tend to remain relatively consistent. For example, in spinal endoscopy surgery, we can systematically characterize the degradation process with a degradation model such as the one formulated in (8). Leveraging this insight, DGGAN is able to achieve reliable and real-time enhancement performance. This implies that, for a specific minimally invasive surgical procedure, it is sufficient to identify and model the major degradation types that are likely to occur. Once this is done, a dedicated enhancement model can be efficiently trained, enabling high-quality and real-time endoscopic video enhancement that directly benefits intraoperative visualization and surgical safety.

4.3 Degradation Representation performance

Degradation representation learning is a key component of our DGGAN framework, as it enables the model to obtain an implicit estimation of endoscopic image degradations, which in turn guides the overall training process. To validate the effectiveness of this learned representation, we performed a visualization analysis.

Specifically, based on the degradation types defined in Table 2, we apply four levels of artificial degradations to high-quality endoscopic images, denoted as L1-L4. These degraded images are then fed into the DAM to extract their degradation representations. To facilitate interpretation, we further project the high-dimensional representations into a two-dimensional space using PCA [51] for visualization. As shown in Fig. 7, the DAM successfully learns meaningful degradation features: different degradation types, such as noise and motion blur, form clearly separable clusters. Even in the case of more complex degradations typical of spinal endoscopic surgery, as modeled in (8), the DAM is still able to capture and distinguish degradation severity to a certain extent, as indicated by the arrow. These results confirm that the DAM provides effective and discriminative degradation representation learning, which forms the basis for robust enhancement performance in diverse surgical scenarios.

4.4 Ablation Study

4.4.1 Effectiveness of the degradation representation

In this study, we investigate the role of degradation representation in our framework. To this end, we remove the pretraining stage of the DAM module in Algorithm 1 (referred to as DGGAN w/o p), which to some extent simulates the vanish of degradation representation learning, and compare it with our full model. The visualization results of the

Table 3: Performance comparison in terms of PSNR (dB), SSIM, parameter counts, FLOPs, and running time (s) of the proposed DGGAN with the SOTAs on the SCARED dataset.

Degradation	Method	PSNR(dB) \uparrow	SSIM \uparrow	Parameters(M) \downarrow	GFLOPs \downarrow	Running time(s) \downarrow
Random Noise	DnCNN	15.50	0.7265	0.56	28.11	0.0205
	CBDNet	28.98	0.8185	4.43	30.84	0.0385
	Uformer	30.96	0.8534	20.63	41.09	0.0419
	Restormer	31.52	0.8710	26.13	108.0	0.5271
	SwinIR	<u>32.76</u>	<u>0.8902</u>	10.89	711.9	11.242
	DGGAN-DAM	33.21	0.9057	4.72	54.41	0.1459
	DGGAN-DRPM	31.03	0.8678	0.63	32.40	0.0291
Motion Blur	DeblurGAN	12.87	0.4879	6.06	26.88	0.0738
	MIMOUNet	17.59	0.6783	6.81	51.26	0.0083
	DBGAN	18.54	0.7121	11.59	74.35	0.1301
	Restormer	<u>23.01</u>	<u>0.8127</u>	26.13	108.0	0.6159
	SwinIR	22.97	0.8094	10.89	711.9	10.855
	DGGAN-DAM	26.86	0.9210	4.72	54.41	0.1421
	DGGAN-DRPM	20.85	0.7785	0.63	32.40	0.0305
Low Light	Zero-DCE	19.11	0.7085	0.024	1.178	0.0018
	RetinexNet	19.16	0.7838	0.56	16.78	2.4734
	EnlightenGAN	19.26	0.7755	54.41	127.45	0.1187
	Restormer	28.83	0.8657	26.13	108.0	0.5764
	SwinIR	25.49	0.8018	10.89	711.9	12.843
	DGGAN-DAM	<u>28.01</u>	<u>0.8619</u>	4.72	54.41	0.1399
	DGGAN-DRPM	26.54	0.8345	0.63	32.40	0.0314
Smoke	DehazeNet	16.86	0.6899	0.02	0.391	0.5237
	FFANet	23.05	0.7311	4.68	231.2	0.3891
	MSBDN	19.01	0.6529	28.71	18.81	0.1031
	Restormer	<u>27.37</u>	<u>0.8346</u>	26.13	108.0	0.6038
	SwinIR	26.79	0.7981	10.89	711.9	11.745
	DGGAN-DAM	28.18	0.8553	4.72	54.41	0.1407
	DGGAN-DRPM	27.13	0.7823	0.63	32.40	0.0276

Table 4: The Evaluation results of NIQE/PIQE on our SES dataset.

	Method	NIQE \downarrow	PIQE \downarrow	Parameters \downarrow
SES	Restormer	4.32	<u>15.79</u>	26.13M
	SwinIR	5.03	18.21	10.89M
	DGGAN-DAM	3.62	13.79	4.72M
	DGGAN-DRPM	<u>3.98</u>	16.82	0.63M

learned degradation representations and the corresponding enhancement performance on the SES dataset are shown in Fig. 8 and Table 5, respectively. Without pretraining, the model almost completely loses its ability to capture meaningful degradation representations, which directly leads to a significant drop in enhancement performance. We attribute this to the fact that, without pretraining, the DAM is treated merely as a generic feature extractor rather than a degradation-oriented encoder, thus losing its capacity to represent degradation effectively.

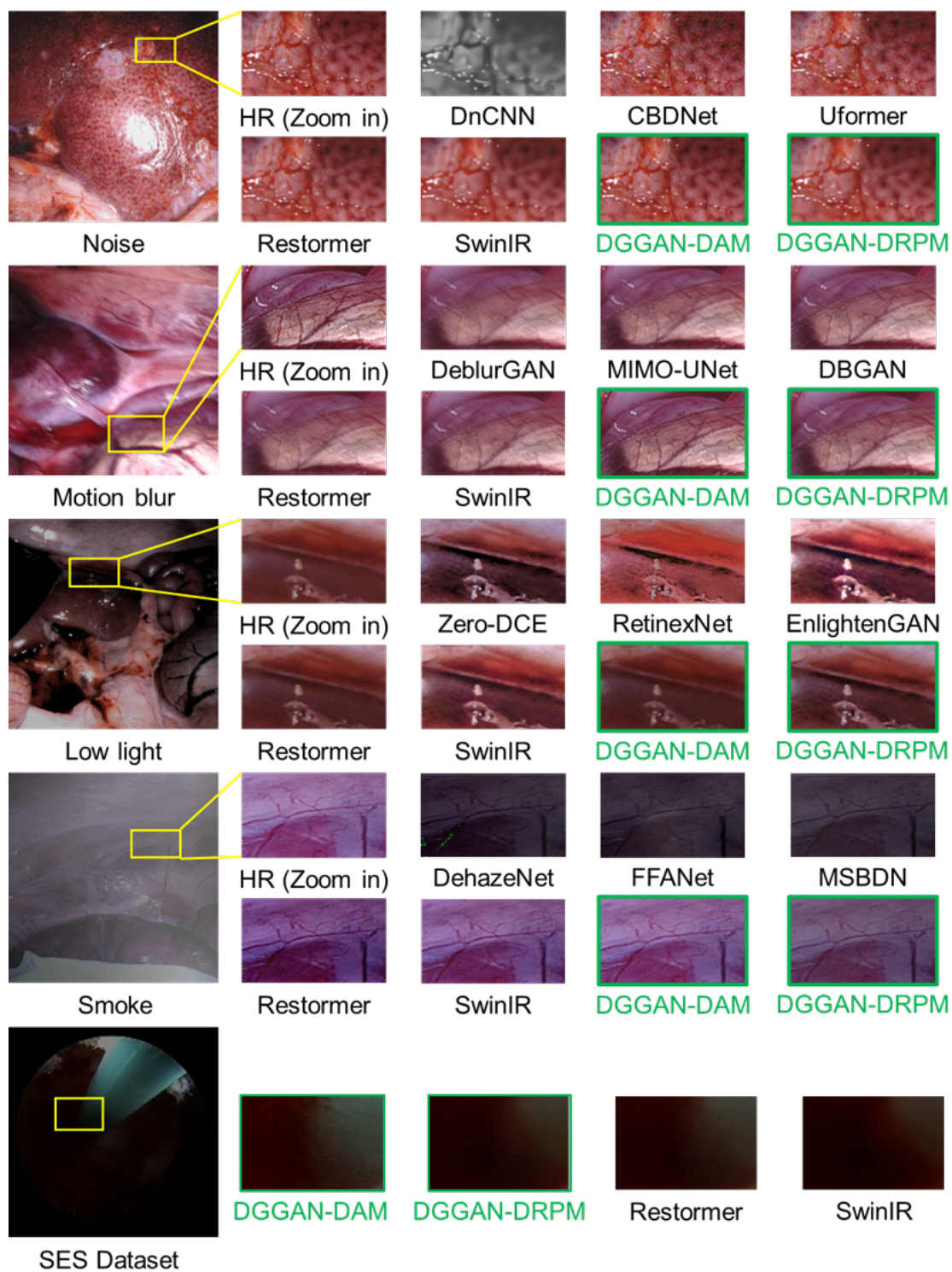


Figure 6: Qualitative comparison of enhancement results on degraded endoscopic datasets. The first four rows correspond to the SCARED dataset under four degradation types: noise, motion blur, smoke, and low light. The last row shows results on our SES dataset.

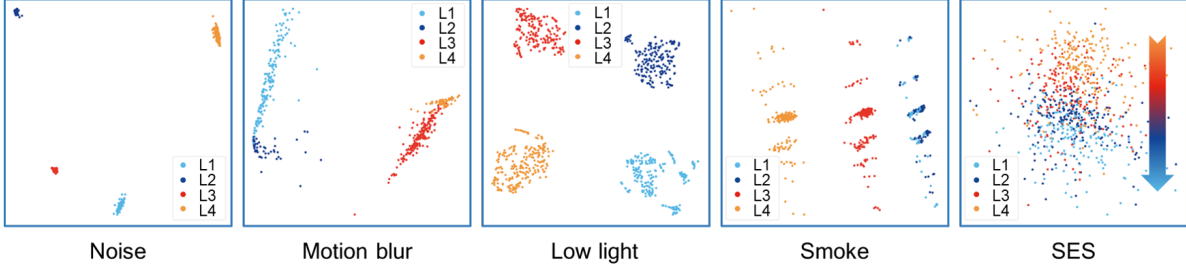


Figure 7: The degradation representation performance of the DAM under different degradation types.

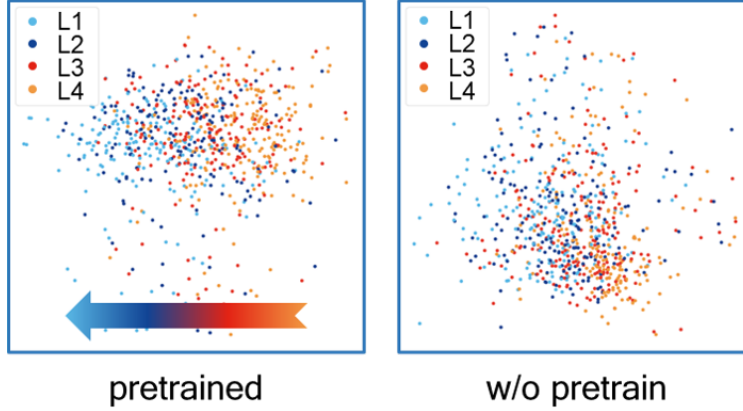


Figure 8: The degradation representation performance on SES dataset with or without pretraining.

Table 5: Enhancement performance with and without DAM pretraining.

Setup	SCARED-noise		SES	
	PSNR \uparrow	SSIM \uparrow	NIQE \downarrow	PIQE \downarrow
DGGAN w/o p	27.21	0.8552	6.19	22.87
DGGAN	33.21	0.9057	3.62	13.79

4.4.2 Effectiveness of the degradation propagation

In this part, we study the impact of different propagation intervals on model performance and inference efficiency. In our default setting, the propagation interval Δ_T is set to 15. To further examine its influence, we test the model with Δ_T values of 3, 5, 10, 20, and 30, and report the average performance and efficiency in Table 6. The results show that smaller Δ_T values yield better enhancement quality but lower inference efficiency, whereas larger Δ_T values achieve the opposite trade-off. This observation is consistent with our intuition: shorter intervals allow more accurate degradation estimation, while longer intervals reduce computational redundancy. Considering that endoscopic videos are typically recorded at 30 fps, we choose $\Delta_T = 15$ as a balance, which ensures satisfactory enhancement quality while maintaining real-time performance.

4.4.3 Effectiveness of the cyclical consistency

In this study, we analyze the contribution of each component in the cyclical consistency loss. As defined in (7), the cyclical loss consists of three terms, L_{cl} , L_{ch} , and L_{cd} . We conduct ablation experiments by removing each of these terms individually and report the results in Table 7. The results show that L_{cl} and L_{ch} have a major impact on the model’s performance, and removing either of them leads to a substantial drop in enhancement quality. In contrast, the role of L_{cd} is relatively minor, as it mainly penalizes inconsistency in degradation representation. Interestingly, removing L_{cd} only slightly affects the final performance, suggesting that the primary benefits of cyclical consistency arise from the content- and quality-level constraints rather than the degradation-level constraint.

Table 6: The enhancement performance under different propagation intervals Δ_T .

Δ_T	SCARED-noise		SES		Running time (s)
	PSNR \uparrow	SSIM \uparrow	NIQE \downarrow	PIQE \downarrow	
3	32.54	0.8844	3.64	14.06	0.0973
5	32.18	0.8803	3.70	14.49	0.0525
10	31.79	0.8776	3.77	15.13	0.0408
15	31.03	0.8678	3.98	16.82	0.0369
20	30.18	0.8595	4.09	17.92	0.0350
30	28.32	0.8391	4.27	19.03	0.0330

Table 7: The effectiveness of the cyclical consistency loss.

Setup	SCARED-noise		SES	
	PSNR \uparrow	SSIM \uparrow	NIQE \downarrow	PIQE \downarrow
w/o L_{cl}	21.53	0.5210	9.38	22.81
w/o L_{ch}	18.87	0.4983	11.01	25.75
w/o L_{cd}	32.77	0.8842	4.03	15.80
Ours	33.21	0.9057	3.62	13.79

5 Conclusion

We developed and validated a novel endoscopic video enhancement framework. Our approach estimates degradation representations of images and propagates them across video frames, thereby enabling high-quality real-time enhancement of endoscopic videos. By achieving a superior balance between performance and efficiency compared with several state-of-the-art methods, our work demonstrates the value of degradation representations in image enhancement. Moreover, this degradation-guided enhancement paradigm implies that, for endoscopic images in a specific minimally invasive surgery, it is sufficient to evaluate and model the potential degradations in order to train an enhancement model, which can then deliver high-quality real-time enhancement during surgery.

Nevertheless, our method has certain limitations. On the one hand, to ensure real-time performance, the parameter size of the single-frame enhancement module was reduced, leading to a performance gap compared with the best-performing state-of-the-art methods. On the other hand, our current design employs a fixed interval for degradation feature estimation, which may limit optimal performance. In future work, we plan to explore a cascaded inference pipeline, where image quality will be monitored in real time to dynamically decide whether degradation estimation is necessary, rather than enforcing estimation at fixed intervals.

Acknowledgments

The National Key Research and Development Program of China supports this work under Grant 2022YFB4703000.

References

- [1] Mingming Pan, Qifan Li, Sucheng Li, Haiqing Mao, Bin Meng, Feng Zhou, and Huilin Yang. Percutaneous endoscopic lumbar discectomy: indications and complications. *Pain physician*, 23(1):49, 2020.
- [2] Sim Kok Swee, Lim Choon Chen, and Tan Sin Ching. Contrast enhancement in endoscopic images using fusion exposure histogram equalization. *Engineering Letters*, 28(3), 2020.
- [3] Wei Tan, Chao Xu, Fang Lei, Qianqian Fang, Ziheng An, Dou Wang, Jubao Han, Kai Qian, and Bo Feng. An endoscope image enhancement algorithm based on image decomposition. *Electronics*, 11(12):1909, 2022.
- [4] Aminou Halidou, Youssoufa Mohamadou, Ado Adamou Abba Ari, and Edinio Jocelyn Gbadoubissa Zacko. Review of wavelet denoising algorithms. *Multimedia Tools and Applications*, 82(27):41539–41569, 2023.
- [5] Qi Yuan and Shengkui Dai. Adaptive histogram equalization with visual perception consistency. *Information Sciences*, 668:120525, 2024.

- [6] Santanu Roy, Kanika Bhalla, and Rachit Patel. Mathematical analysis of histogram equalization techniques for medical image enhancement: a tutorial from the perspective of data loss. Multimedia Tools and Applications, 83(5):14363–14392, 2024.
- [7] Shiyu Yang, Tai Guo, and Ruoya Zhan. Capsule endoscopy image deblurring method based on multi-scale recurrent network. In Journal of Physics: Conference Series, volume 2640, page 012003. IOP Publishing, 2023.
- [8] Xiaowei Song, Hui Tang, Chunfeng Yang, Guangquan Zhou, Yangang Wang, Xinjun Huang, Jie Hua, Gouenou Coatrieux, Xiaopu He, and Yang Chen. Deformable transformer for endoscopic video super-resolution. Biomedical Signal Processing and Control, 77:103827, 2022.
- [9] Wenfeng Huang, Xiangyun Liao, Hao Chen, Ying Hu, Wenjing Jia, and Qiong Wang. Deep local-to-global feature learning for medical image super-resolution. Computerized Medical Imaging and Graphics, 115:102374, 2024.
- [10] Lingbing Peng, Shuaicheng Liu, Dehua Xie, Shuyuan Zhu, and Bing Zeng. Endoscopic video deblurring via synthesis. In 2017 IEEE Visual Communications and Image Processing (VCIP), pages 1–4. IEEE, 2017.
- [11] Kevin Tchaka, Vijay M Pawar, and Danail Stoyanov. Chromaticity based smoke removal in endoscopic images. In Medical Imaging 2017: Image Processing, volume 10133, pages 463–470. SPIE, 2017.
- [12] Jinzhao Lin, Meiqiu Jiang, Yu Pang, Huiqian Wang, Zhu Chen, Chongyuan Yan, Qinghui Liu, and Yuanfa Wang. A desmoking algorithm for endoscopic images based on improved u-net model. Concurrency and Computation: Practice and Experience, 33(22):e6320, 2021.
- [13] Shaofeng Zou, Mingzhu Long, Xuyang Wang, Xiang Xie, Guolin Li, and Zhihua Wang. A cnn-based blind denoising method for endoscopic images. In 2019 IEEE Biomedical Circuits and Systems Conference (BioCAS), pages 1–4. IEEE, 2019.
- [14] JJ Wu, Yang Yuan, Long Liu, Haipo Cui, Tianying Xu, Miao Zhou, Zhanheng Chen, and Bing Xu. Research progress of frontier image processing in medi-cal endoscopes. Prog. Med. Devices, 1(2):62–77, 2023.
- [15] Qian Wang, Ning Pan, Wei Xiong, Heng Lu, Nan Li, and Xijing Zou. Reduction of bubble-like frames using a rss filter in wireless capsule endoscopy video. Optics & Laser Technology, 110:152–157, 2019.
- [16] Yasin Almalioglu, Kutsev Bengisu Ozyoruk, Abdulkadir Gokce, Kagan Incetan, Guliz Irem Gokceler, Muhammed Ali Simsek, Kivanc Ararat, Richard J Chen, Nicholas J Durr, Faisal Mahmood, et al. Endol2h: deep super-resolution for capsule endoscopy. IEEE Transactions on Medical Imaging, 39(12):4297–4309, 2020.
- [17] Tianyi Zhang and Jie Yang. Transformer with hybrid attention mechanism for stereo endoscopic video super resolution. Symmetry, 15(10):1947, 2023.
- [18] Mansoor Hayat and Supavadee Aramvith. E-sevsr—edge guided stereo endoscopic video super-resolution. IEEE Access, 12:30893–30906, 2024.
- [19] Mansoor Hayat, Supavadee Aramvith, and Titipat Achakulvisut. Combined channel and spatial attention-based stereo endoscopic image super-resolution. In TENCON 2023-2023 IEEE Region 10 Conference (TENCON), pages 920–925. IEEE, 2023.
- [20] Mansoor Hayat and Supavadee Aramvith. Saliency-aware deep learning approach for enhanced endoscopic image super-resolution. IEEE Access, 12:83452–83465, 2024.
- [21] Ziheng An, Chao Xu, Kai Qian, Jubao Han, Wei Tan, Dou Wang, and Qianqian Fang. Eien: endoscopic image enhancement network based on retinex theory. Sensors, 22(14):5464, 2022.
- [22] Yifan Jiang, Xinyu Gong, Ding Liu, Yu Cheng, Chen Fang, Xiaohui Shen, Jianchao Yang, Pan Zhou, and Zhangyang Wang. Enlightengan: Deep light enhancement without paired supervision. IEEE transactions on image processing, 30:2340–2349, 2021.
- [23] LinJie Guo, Xiao Xiao, ChunCheng Wu, Xianhui Zeng, Yuhang Zhang, Jiang Du, Shuai Bai, Jia Xie, Zhiwei Zhang, Yuhong Li, et al. Real-time automated diagnosis of precancerous lesions and early esophageal squamous cell carcinoma using a deep learning model (with videos). Gastrointestinal endoscopy, 91(1):41–51, 2020.
- [24] Masayoshi Yamada, Yutaka Saito, Hitoshi Imaoka, Masahiro Saiko, Shigemi Yamada, Hiroko Kondo, Hiroyuki Takamaru, Taku Sakamoto, Jun Sese, Aya Kuchiba, et al. Development of a real-time endoscopic image diagnosis support system using deep learning technology in colonoscopy. Scientific reports, 9(1):14465, 2019.
- [25] Meilu Zhu, Zhen Chen, and Yixuan Yuan. Dsi-net: Deep synergistic interaction network for joint classification and segmentation with endoscope images. IEEE Transactions on Medical Imaging, 40(12):3315–3325, 2021.
- [26] Hemalatha Gunasekaran, Krishnamoorthi Ramalakshmi, Deepa Kanmani Swaminathan, and Manuel Mazzara. Git-net: an ensemble deep learning-based gi tract classification of endoscopic images. Bioengineering, 10(7):809, 2023.

- [27] Zihan Nie, Muhao Xu, Zhiyong Wang, Xiaoqi Lu, and Weiye Song. A review of application of deep learning in endoscopic image processing. *Journal of Imaging*, 10(11):275, 2024.
- [28] Jun-Yan Zhu, Taesung Park, Phillip Isola, and Alexei A Efros. Unpaired image-to-image translation using cycle-consistent adversarial networks. In *Proceedings of the IEEE international conference on computer vision*, pages 2223–2232, 2017.
- [29] Kaiming He, Haoqi Fan, Yuxin Wu, Saining Xie, and Ross Girshick. Momentum contrast for unsupervised visual representation learning. In *Proceedings of the IEEE/CVF conference on computer vision and pattern recognition*, pages 9729–9738, 2020.
- [30] Longguang Wang, Yingqian Wang, Xiaoyu Dong, Qingyu Xu, Jungang Yang, Wei An, and Yulan Guo. Unsupervised degradation representation learning for blind super-resolution. In *Proceedings of the IEEE/CVF conference on computer vision and pattern recognition*, pages 10581–10590, 2021.
- [31] Aaron van den Oord, Yazhe Li, and Oriol Vinyals. Representation learning with contrastive predictive coding. *arXiv preprint arXiv:1807.03748*, 2018.
- [32] Ze Liu, Yutong Lin, Yue Cao, Han Hu, Yixuan Wei, Zheng Zhang, Stephen Lin, and Baining Guo. Swin transformer: Hierarchical vision transformer using shifted windows. In *Proceedings of the IEEE/CVF international conference on computer vision*, pages 10012–10022, 2021.
- [33] Max Allan, Jonathan Mcleod, Congcong Wang, Jean Claude Rosenthal, Zhenglei Hu, Niklas Gard, Peter Eisert, Ke Xue Fu, Trevor Zeffiro, Wenyao Xia, et al. Stereo correspondence and reconstruction of endoscopic data challenge. *arXiv preprint arXiv:2101.01133*, 2021.
- [34] Syed Waqas Zamir, Aditya Arora, Salman Khan, Munawar Hayat, Fahad Shahbaz Khan, and Ming-Hsuan Yang. Restormer: Efficient transformer for high-resolution image restoration. In *Proceedings of the IEEE/CVF conference on computer vision and pattern recognition*, pages 5728–5739, 2022.
- [35] Jingyun Liang, Jiezhang Cao, Guolei Sun, Kai Zhang, Luc Van Gool, and Radu Timofte. Swinir: Image restoration using swin transformer. In *Proceedings of the IEEE/CVF international conference on computer vision*, pages 1833–1844, 2021.
- [36] Jiwon Kim, Jung Kwon Lee, and Kyoung Mu Lee. Accurate image super-resolution using very deep convolutional networks. In *Proceedings of the IEEE conference on computer vision and pattern recognition*, pages 1646–1654, 2016.
- [37] Wei-Sheng Lai, Jia-Bin Huang, Narendra Ahuja, and Ming-Hsuan Yang. Deep laplacian pyramid networks for fast and accurate super-resolution. In *Proceedings of the IEEE conference on computer vision and pattern recognition*, pages 624–632, 2017.
- [38] Anish Mittal, Rajiv Soundararajan, and Alan C Bovik. Making a “completely blind” image quality analyzer. *IEEE Signal processing letters*, 20(3):209–212, 2012.
- [39] Narasimhan Venkatanath, D Praneeth, S Channappayya Sumohana, S Medasani Swarup, et al. Blind image quality evaluation using perception based features. In *2015 twenty first national conference on communications (NCC)*, pages 1–6. IEEE, 2015.
- [40] Kai Zhang, Wangmeng Zuo, Yunjin Chen, Deyu Meng, and Lei Zhang. Beyond a gaussian denoiser: Residual learning of deep cnn for image denoising. *IEEE transactions on image processing*, 26(7):3142–3155, 2017.
- [41] Shi Guo, Zifei Yan, Kai Zhang, Wangmeng Zuo, and Lei Zhang. Toward convolutional blind denoising of real photographs. In *Proceedings of the IEEE/CVF conference on computer vision and pattern recognition*, pages 1712–1722, 2019.
- [42] Zhendong Wang, Xiaodong Cun, Jianmin Bao, Wengang Zhou, Jianshuang Liu, and Houqiang Li. Uformer: A general u-shaped transformer for image restoration. In *Proceedings of the IEEE/CVF conference on computer vision and pattern recognition*, pages 17683–17693, 2022.
- [43] Orest Kupyn, Volodymyr Budzan, Mykola Mykhailych, Dmytro Mishkin, and Jiří Matas. Deblurgan: Blind motion deblurring using conditional adversarial networks. In *Proceedings of the IEEE conference on computer vision and pattern recognition*, pages 8183–8192, 2018.
- [44] Sung-Jin Cho, Seo-Won Ji, Jun-Pyo Hong, Seung-Won Jung, and Sung-Jea Ko. Rethinking coarse-to-fine approach in single image deblurring. In *Proceedings of the IEEE/CVF international conference on computer vision*, pages 4641–4650, 2021.
- [45] Kaihao Zhang, Wenhan Luo, Yiran Zhong, Lin Ma, Bjorn Stenger, Wei Liu, and Hongdong Li. Deblurring by realistic blurring. In *Proceedings of the IEEE/CVF conference on computer vision and pattern recognition*, pages 2737–2746, 2020.

- [46] Chunle Guo, Chongyi Li, Jichang Guo, Chen Change Loy, Junhui Hou, Sam Kwong, and Runmin Cong. Zero-reference deep curve estimation for low-light image enhancement. In Proceedings of the IEEE/CVF conference on computer vision and pattern recognition, pages 1780–1789, 2020.
- [47] Chen Wei, Wenjing Wang, Wenhan Yang, and Jiaying Liu. Deep retinex decomposition for low-light enhancement. arXiv preprint arXiv:1808.04560, 2018.
- [48] Bolun Cai, Xiangmin Xu, Kui Jia, Chunmei Qing, and Dacheng Tao. Dehazenet: An end-to-end system for single image haze removal. IEEE transactions on image processing, 25(11):5187–5198, 2016.
- [49] Xu Qin, Zhilin Wang, Yuanchao Bai, Xiaodong Xie, and Huizhu Jia. Ffa-net: Feature fusion attention network for single image dehazing. In Proceedings of the AAAI conference on artificial intelligence, volume 34, pages 11908–11915, 2020.
- [50] Hang Dong, Jinshan Pan, Lei Xiang, Zhe Hu, Xinyi Zhang, Fei Wang, and Ming-Hsuan Yang. Multi-scale boosted dehazing network with dense feature fusion. In Proceedings of the IEEE/CVF conference on computer vision and pattern recognition, pages 2157–2167, 2020.
- [51] Hervé Abdi and Lynne J Williams. Principal component analysis. Wiley interdisciplinary reviews: computational statistics, 2(4):433–459, 2010.